THE JOURNAL OF PHYSICAL CHEMISTRY B

Article

pubs.acs.org/JPCB

Dynamics of Phenanthrenequinone on Carbon Nano-Onion Surfaces Probed by Quasielastic Neutron Scattering

Suresh M. Chathoth,*[,†] Daniela M. Anjos,[‡] Eugene Mamontov,[†] Gilbert M. Brown,[‡] and Steven H. Overbury[‡]

[†]Chemical and Engineering Materials Division, Neutron Scattering Directorate, Oak Ridge National Laboratory, Oak Ridge, Tennessee 37831, United States

[‡]Chemical Sciences Division, Oak Ridge National Laboratory, Oak Ridge, Tennessee 37831, United States

ABSTRACT: We used quasielastic neutron scattering (QENS) to study the dynamics of phenanthrenequinone (PQ) on the surface of onion-like carbon (OLC), or so-called carbon onions, as a function of surface coverage and temperature. For both the high- and low-coverage samples, we observed two diffusion processes; a faster process and nearly an order of magnitude slower process. On the high-coverage surface, the slow diffusion process is of long-range translational character, whereas the fast diffusion process is spatially localized on the length scale of ~4.7 Å. On the low-coverage surface, both diffusion processes are spatially localized; on the same length scale of ~4.7 Å for the fast diffusion and a somewhat larger length scale for the slow diffusion. Arrhenius temperature dependence is observed except for the long-range diffusion on the high-coverage surface. We attribute the fast diffusion process to the generic localized in-cage dynamics of PQ molecules, and the slow diffusion process to the long-range translational dynamics of PQ molecules, which, depending on the coverage, may be either spatially restricted or long-range. On the low-coverage surface, uniform surface coverage is not attained, and the PQ molecules experience the effect of spatial constraints on their long-range translational dynamics. Unexpectedly, the dynamics of PQ molecules on OLC as a function of temperature and surface coverage bears qualitative resemblance to the dynamics of water molecules on oxide surfaces, including practically temperature-independent residence times for the low-coverage surface. The dynamics features that we observed may be universal across different classes of surface adsorbates.

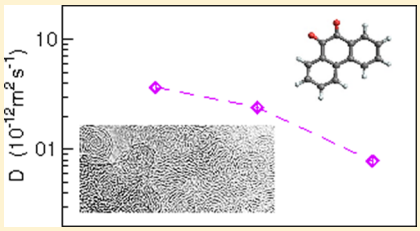

INTRODUCTION

Proton-coupled electron transfer (PCET) reactions play an important role in a broad range of energy conversion processes, e.g., in many types of solar cells, fuel cells, and other electrochemical devices.[1,2] Recent advances in the theory of PCET enable the prediction of the impact of system properties on the reaction rate. Elucidating the mechanism of PCET reactions on the surface of interest would facilitate design of better materials and interfaces for improvement of alternative energy production.[3] Attaching redox molecules to a conductive surface is conveniently used in the studies of the electron transfer kinetics. A large number of devices related to the conversion and storage of energy use carbon with different morphologies and sizes (mesoporous, nanotubes, graphene, onions, etc). High surface area carbon is of interest as a support material or electrode for applications in catalysis, electrocatalysis, and photocatalysis.[4] Several parameters have to be taken into account when aiming at deciphering electron transfer kinetics through a molecularly adsorbed monolayer, e.g., the adsorption geometry of the redox couple, possible clustering of the redox molecules, and the effects of the chain length and bridging structure.[3] The nature of the adsorption can strongly affect the electron transfer kinetics. The mobility of an adsorbed molecule will cause a deviation of the experimental rate constant value due to a surface reaction parallel to the heterogeneous reaction.[5] Although there are studies of diffusion of weakly adsorbed molecules in porous oxide supports,[6] there is no experimental information about the dynamics of redox molecules, particularly phenanthrenequinone (PQ), on large surface area materials such as onion-like carbon (OLC). OLC are quasi-spherical nanoparticles consisting of concentric graphitic shells (see Figure 1b inset) with a specific surface area of ~500 $m^2\ g^{-1}$.[7] In this study, we have investigated the microscopic diffusivity of PQ on OLC surface as a function of surface coverage and temperature using quasielastic neutron scattering (QENS).

MATERIALS AND METHODS

Pure OLC samples were obtained from Professor Gogotsi's group at Drexel University, and the details of OLC synthesis were described elsewhere.[8] The OLC powders were dried in a vacuum oven at 60 °C for 12 h and loaded into the Al sample holder. 9,4-Phenanthrenequinone or $C_{14}H_8O_2$ (PQ) with a purity of 99.99% was procured from Alfa Aesar. Molecular structure of PQ is shown in the Figure 1a inset. PQ is solid at room temperature, and its melting and boiling points are 211 and 360 °C, respectively. The PQ-modified OLC were obtained in two concentrations by soaking the carbon in 5 and 1.5×10^{-3} mol/L PQ dissolved in methanol. The OLC powder was soaked in the

Received: March 5, 2012
Revised: May 17, 2012
Published: May 30, 2012

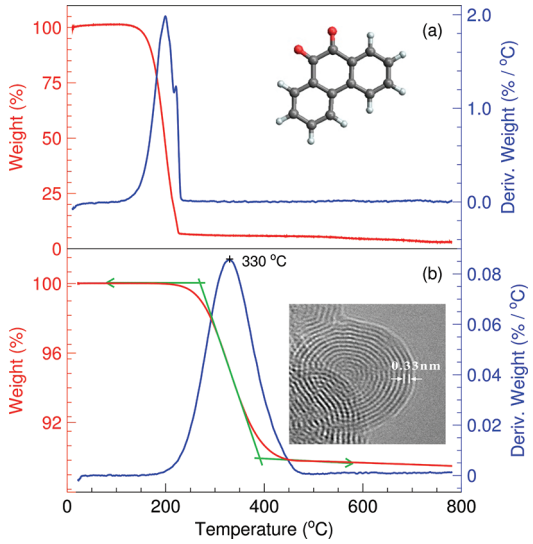

Figure 1. (a) TGA curves for bulk PQ. Inset: a molecular structure of PQ; the red, black, and white balls represents oxygen, carbon, and hydrogen atoms, respectively. (b) TGA curve for the PQ adsorbed on carbon nano-onions in N_2 atmosphere, 10 mL/min, 10 °C/min. Inset: a transmission electron microscopic image of carbon nano-onions (micrograph courtesy Professor Gogotsi's group, Drexel University).

PQ solution for 20 min and then filtered using a 0.2 μm PTFE (Teflon) filter. The sample was transferred to a quartz tube and heated at 60 °C for 12 h in a vacuum furnace to get rid of methanol. The samples were loaded and sealed in the sample holders for neutron scattering experiments in an inert atmosphere to avoid water adsorption from the atmosphere. Thermo-gravimetric analyses (TGA) were carried out using a Q500 from TA Instruments. Samples of typically 20 mg were placed in Pt pans and heated from 25 to 800 at 10 °C/min, under flowing N_2 atmosphere. Thermo-gravimetric analyses (TGA) show a peak at different temperatures in the derivative weight removal curves for the bulk PQ and PQ-modified OLCs (Figure 1a,b). A difference of more than 100 °C indicates the adsorption of the PQ molecule on carbon substrate. The desorption temperatures are rather similar but slightly higher for the lower PQ coverage (338 °C) (Table 1). The measured weight loss and the surface area of the OLC were used to calculate the PQ coverage on carbon onions. The results are listed in Table 1.

Table 1. Temperature of Desorption Peaks and Surface Coverage of PQ on Carbon Nano-Onion

sample	T peak (°C)	mass loss (%)	coverage (molecules/nm^2)
neat PQ	210	100.0	
PQ/C high coverage	330	10.4	0.60
PQ/C low coverage	338	4.8	0.23

The neutron scattering experiments were performed on the backscattering spectrometer (BASIS) at the Spallation Neutron Source, Oak Ridge National Laboratory.[9] For the chosen experimental setup, the wavelength, the energy resolution at the elastic line, and the momentum transfer range were λ = 6.267 Å, 3.4 μeV, and 0.2 Å^{-1} to 2.0 Å^{-1}, respectively. In this study, the data analysis was limited to a dynamic range of ±100 μeV, which is free from spurious scattering. The data were collected at five different temperatures, T = 290, 310, 330, 340, and 350 K. The dry carbon loaded in the similar sample holder was also measured at each temperature. The data collected at 15 K were used as the resolution function. The dynamic structure factor, $S(Q,\omega)$, was deduced by normalizing the raw data to the vanadium standard, correcting for the dry OLC and container scattering, and interpolating to constant values of the momentum transfer, Q. Since PQ contains eight hydrogen atoms in a single molecule, the QENS signal originates mainly from the incoherent scattering by these hydrogen atoms. Hence, Fourier transformation of $S(Q,\omega)$ with subsequent normalization to unity at t = 0 yields the self-correlation intermediate scattering function, $I(Q,t)/I(Q,0)$. Below 310 K, the quasi-elastic broadening was not detectable, indicating that the dynamics of PQ on OLC surfaces was slower than the energy resolution limit of the BASIS (about a nanosecond). Hence, further analysis of the QENS spectra was limited to 330, 340, and 350 K.

RESULTS AND DISCUSSION

There is a significant elastic scattering from the OLC matrix that gives rise to elastic peak over the quasielastic intensity in the dynamic structure factor, $S(Q,\omega)$. Upon Fourier transformation, this extra elastic intensity gives rise to a flat background in the intermediate scattering function. As one can see from Figure 2,

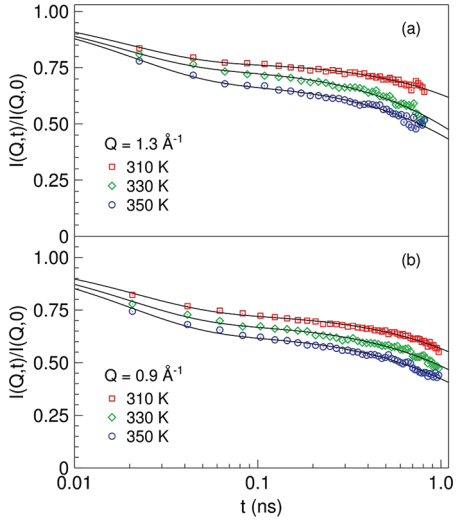

Figure 2. Self-correlation intermediate scattering function of PQ on CNO surface at three different temperatures (a) for the high-coverage sample at a Q value of 1.3 Å^{-1} and (b) for the low-coverage sample at a Q value of 0.9 Å^{-1}. The solid lines are the fit with eq 1.

the $I(Q,t)/I(Q,0)$ curves cannot be described by a single exponential decay, and models with an exponential decay plus a background were not successful in fitting the data either. However, fits with two exponential terms plus a background (eq 1)

$$\frac{I(Q,t)}{I(Q,0)} = \left[A_1(Q)\exp\left(-\frac{t}{\tau_1(Q)}\right) + A_2(Q)\exp\left(-\frac{t}{\tau_2(Q)}\right)\right] + B(Q) \quad (1)$$

can describe the data well at all Q values and temperatures. Here, $\tau_1(Q)$ and $\tau_2(Q)$ are the relaxation times associated with the fast and slow dynamics components, $A_1(Q)$ and $A_2(Q)$ are the respective Q-dependent spectral weights, and $B(Q)$ is the background. The data fitted with eq 1 are shown in Figure 2 for

dx.doi.org/10.1021/jp302155a | J. Phys. Chem. B 2012, 116, 7291−7295

the high-coverage and low-coverage samples at a Q value of 1.3 Å^{-1} and 0.9 Å^{-1}, respectively, for the three measured temperatures. The model fits the data well for both samples. From these fits, we obtained the relaxation times at each Q value and their temperature dependence. Since there is a broad Bragg's peak due to OLC centered at a Q value of 1.5 Å^{-1}, we limited the data analysis to Q values not exceeding 1.3 Å^{-1}. The inverse relaxation time for the fast process is plotted against Q^2 in Figure 3a for the high-coverage sample. The Q^2 dependence of the $1/\tau$

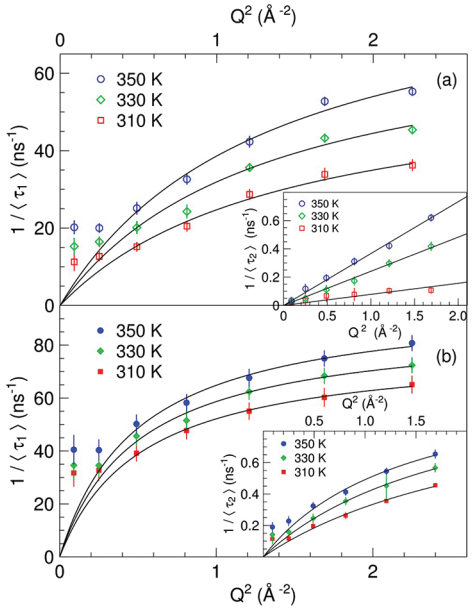

Figure 3. (a) High-coverage sample: inverse relaxation time, τ_1, is plotted against the square of momentum transfer, Q^2, and the lines are the fits with jump diffusion model (eq 3). Inset: inverse relaxation time, τ_2, is plotted against the square of momentum transfer, Q^2. The lines are the fits with the continuous diffusion model (eq 2). (b) Similar plots for the low-coverage sample; here, the inverse of both τ_1 and τ_2 are fitted with the jump diffusion model (eq 3).

exhibits jump diffusion behavior. For $Q < 0.7$ Å^{-1}, the values of the $1/\tau$ are nearly invariant, indicating that the fast diffusion process is spatially confined. However, the slow process does not exhibit jump diffusion behavior but instead shows continuous diffusion with a linear dependence of $1/\tau$ on the Q^2 and no signs of spatial confinement in the low Q data (see inset in Figure 3a). The diffusion coefficients, D, can be obtained from the Q-dependence of the QENS broadening, $1/\tau(Q)$, as follows:[10]

$$\frac{1}{\tau(Q)} = DQ^2 \tag{2}$$

$$\frac{1}{\tau(Q)} = \frac{1}{\tau_0}\left[1 - \frac{1}{1 + DQ^2\tau_0}\right] \tag{3}$$

where eqs 2 and 3 represent the diffusivity for the continuous and the jump diffusion processes, respectively. Here, $\tau(Q)$ represents the Q-dependent relaxation time, and τ_0 is the residence time between the successive jumps (applicable only to a jump diffusion, but not continuous diffusion process). For the low-coverage sample, the relaxation times for both the fast and the slow process exhibit jump diffusion behavior, similar to the fast diffusion process in the high-coverage sample but different from the slow diffusion process in that sample. As we have mentioned, the latter exhibits continuous diffusion, not jump diffusion. For the low-coverage sample, both the fast and slow diffusion processes are spatially constrained, as indicated by the flat relaxation times at the low Q values (see Figure 3b). It should be noted, however, that the spatial confinement for the slow diffusion process is less pronounced compared to the fast diffusion process, as indicated by the relatively lower Q values where the relaxation times exhibit a plateau. In the next paragraphs, we will discuss how the quantitative information on the spatial constrains of the diffusion processes can be extracted from the data.

The self-diffusion coefficient can be, in principle, calculated using eq 2 (continuous diffusion) for the slow process in the high-coverage sample and eq 3 (jump diffusion) for the other processes; that is, the fast process in the high-coverage sample and both fast and slow processes in the low-coverage sample. However, in the presence of spatial confinement, the more meaningful parameter is the residence time between jumps, τ_0, in eq 3. This is because the diffusion coefficient for the spatially restricted processes should not be determined from eq 3, which assumes normal diffusion behavior, that is, the QENS broadening that approaches zero in the limit of low Q. Instead, the QENS broadening for the spatially restricted process tends to plateau at some value Γ below a certain value of Q_0. Then, the confinement radius, a, and the diffusion coefficient, D, for the confined process can be evaluated as $a = 3.3/Q_0$ and $D = (\Gamma/\hbar)a^2/4.33$, where $\hbar$ is the reduced Planck's constant.[11−13] Qualitative estimate of the Q_0 is easy to obtain from the plots shown in Figure 3, but more precise determination of the Q_0 is difficult, thus rendering the so determined values of the diffusion coefficient D less reliable. However, the residence time τ_0 is obtained from the fits with good precision; besides, the value of τ_0 is not affected by the presence or absence of confinement effects, unlike the value of D. Therefore, Figure 4 displays inverse residence times for the spatially restricted dynamic components.

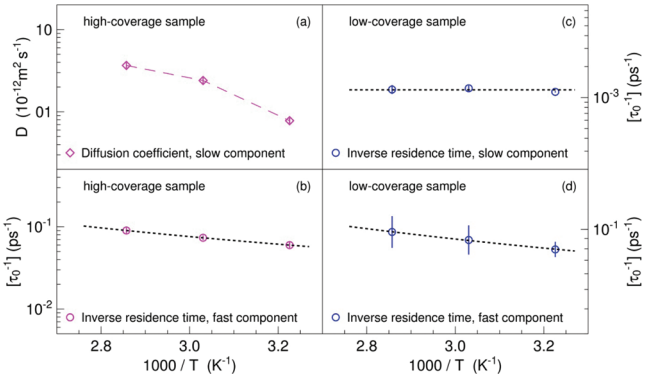

Figure 4. (a) Diffusion coefficient for the slow process in the high-coverage sample. (b) Inverse residence time for the fast process in the high-coverage sample. (c) Inverse residence time for the slow process in the low-coverage sample. (d) Inverse residence time for the fast process in the low-coverage sample. When not visible, the error bars are within the symbols.

Among the four processes shown in Figure 4, only the slow diffusivity for the high-coverage sample (which also, uniquely, gives rise to continuous diffusion rather than jump diffusion and shows no signs of spatial confinement in the low Q data) displays an appreciable sign of non-Arrhenius temperature dependence (see inset in Figure 4a). The non-Arrhenius behavior of the diffusivity is usually present in bulk liquids that are fragile glass-

dx.doi.org/10.1021/jp302155a | J. Phys. Chem. B 2012, 116, 7291−7295

formers.[14] It has been shown that microscopic diffusion dynamics of, e.g., hydration water on an oxide surface, starts exhibiting qualitatively bulk-like behavior, including non-Arrhenius temperature dependence of the relaxation times, with increasing hydration level (that is, increasing surface coverage).[15] Furthermore, in such a relatively high-coverage state, water on an oxide surface exhibits long-range translational diffusivity.[16] Thus, our data indicate that the PQ molecules on the carbon onion surface in the low-coverage sample likely do not form continuous surface coverage. Neither long-range translational diffusivity, nor super-Arrhenius temperature dependence of the relaxation times, which requires a well-formed network of molecules, can be observed.

Using the estimate of $a = 3.3/Q_0$, as discussed above, with $Q_0 = 0.7$ Å^{-1}, we arrived at a value of $a = 4.7$ Å for the radius of the spatial localization of the fast diffusion process for both high-coverage and low-coverage samples. As for the spatial localization of the slow diffusion process in the low-coverage sample, the estimate using $Q_0 = 0.5$ Å^{-1}, gives the radius of $a = 6.6$ Å. Likewise, for the slow diffusion process in the high-coverage sample, from the fact that there is no plateau in the Q-dependence of the data down to at least 0.3 Å^{-1}, we can conclude that there is no localization for this process up to at least $(2 \times 3.3/0.3$ Å$^{-1}) = 22$ Å length scale. Even if the confinement effects on a larger length scale were present, we would be unable to observe them in the Q-range of our experiment.

From the data in Table 1, we see that each molecule occupies an area of 1.7 nm^2 and 4.3 nm^2 in high- and low-coverage samples, respectively. The effective area of the PQ molecule is about 0.9 nm^2. Therefore, the following picture of the diffusion processes emerges. Let us start from the high-coverage sample. The characteristic dimensions of the molecule and the intermolecular distance are 9.5 Å and 13 Å, respectively. The localization radius of 4.7 Å for the faster process then suggests that this faster process is related to the molecule rattling in the cage made by the nearest neighbors. The case itself is not static; this gives rise to the fast in-cage process that, while spatially restricted, still involves significant center-of-mass motions and therefore yields the Q-dependent scattering signal with jump diffusion appearance at higher Q values. The slow process in the high-coverage sample is the long-range translational diffusion associated with the cage breaking. Because the surface coverage is continuous (that is, the cages are connected across the surface), this leads to the long-range translational diffusion with its characteristic Q-dependence of the scattering signal.

In the low-coverage sample, the characteristic intermolecular distance that one would calculate from Table 1 assuming the uniform distribution of molecules over the surface is 21 Å. Thus, in the case of the uniform distribution of PQ molecules, one could expect a different (much less spatially restricted) fast process and the slow process that is still of long-range character. However, the data from the low-coverage sample tell a very different story. Compared to the high-coverage sample, the cage made of the neighboring molecules remains unchanged. Instead, there is a disruption of the long-range diffusion process. Therefore, we have to conclude that the surface coverage in the low-coverage sample is not uniform. The clusters of molecules still form cages, thereby yielding the same fast in-cage dynamics, but these clusters are now separated and no longer form a continuous surface network. Thus, instead of the slow process due to the long-range translational diffusion, we now have a slow process that is spatially restricted; the cage breaking still occurs within the clusters of molecules, but it does not lead to long-range diffusion because the clusters do not form continuous surface coverage.

While there is a qualitative difference in the slow diffusion processes between the low-coverage sample (spatially restricted) and high-coverage sample (unrestricted, at least on the length scale of the neutron probe), the fast diffusion processes does not change as dramatically as a function of coverage. This is because, regardless of the coverage, the fast process originates from the motions localized in the effective transient cage made by the nearest neighbor molecules,[17−21] and, as such, is always spatially restricted by the size of this cage. As we have already mentioned, similar to the slow process, the fast process is related to the motions of the molecular center of mass. Such a localized fast process can actually be universal across glass-forming systems of small molecules.[22] Therefore; the fast process originates from the in-cage center-of-mass motion of PQ molecules. We have verified that there is no QENS signal, besides the elastic line, from a bulk PQ sample measured on the BASIS, up to a highest temperature of 350 K.

The temperature dependence of the inverse residence time shows Arrhenius behavior for the fast process on the low- and high-coverage surfaces, with activation energy of 4.5 and 9.2 kJ/mol, respectively. As one can see from Figure 4c, the inverse residence times obtained for the slow diffusion on the low-coverage surface show practically no temperature dependence. This bears a striking resemblance to the behavior of water molecules on an oxide surface at low coverage observed by QENS and molecular dynamic simulations.[15]

Quite unexpectedly, PQ on CNO shows dynamic behavior qualitatively similar to that of water on oxide surfaces.[15,16] This result may indicate some universal dynamics features common across different classes of surface adsorbates, which present themselves as follows. At low surface coverage (until the continuous coverage is attained), the translational dynamics of surface molecules remains spatially confined, rather than long-range, with very weak, if any, temperature dependence. Once the continuous surface coverage is attained, the translational dynamics becomes of long-range character, while its temperature dependence is non-Arrhenius, due to the presence of an extensive network of molecules. Regardless of the surface coverage, high or low, there exists a comparatively faster dynamic component originating from the generic in-cage dynamics of molecules, which is relatively insensitive to the degree of the surface coverage because of its predominant dependence on the transient cage formed by the nearest neighbors.

CONCLUSIONS

In conclusion, we have studied PQ dynamics on carbon nano-onion surfaces as a function of the surface coverage and temperature. On both the low- and high-coverage surfaces, we observed two diffusion processes, a faster and a slower, both of translational character, even though in most cases they are spatially confined. In particular, the faster diffusion process in both samples is spatially confined within a radius of about 4.7 Å. We attribute this process to the generic in-cage dynamics of molecules, which predominantly depends on the transient cage formed by the nearest neighbors and thus is relatively insensitive to the degree of the surface coverage. The slower process is due to long-rage translational diffusion and is either spatially restricted (in the low-coverage sample) or unrestricted (in the high-coverage sample, where continuous surface coverage is attained). Among all the observed processes, only the slow diffusivity for the high-coverage sample (which also, uniquely,

gives rise to continuous diffusion rather than jump diffusion and shows no signs of spatial confinement in the low Q data) displays non-Arrhenius temperature dependence. Surprisingly, PQ on CNO shows dynamic behavior qualitatively similar to that of water on oxide surfaces, which may be indicative of the universal features in the dynamics of surface adsorbates.

AUTHOR INFORMATION

Corresponding Author

*E-mail: mavilachaths@ornl.gov.

Notes

The authors declare no competing financial interest.

ACKNOWLEDGMENTS

This research is based upon work supported as part of the Fluid Interface Reactions, Structures, and Transport (FIRST) Center, an Energy Frontier Research Center funded by the U.S. Department of Energy, Office of Science, Office of Basic Energy Sciences. The neutron scattering studies were conducted with support from the Scientific User Facilities Division, Office of Basic Energy Sciences, U.S. DOE. Oak Ridge National Laboratory is managed by UT-Battelle, LLC, for U.S. DOE under Contract No. DE-AC05-00OR22725.

REFERENCES

(1) Brodd, R. J.; Bullock, K. R.; Leising, R. A.; Middaugh, R. L.; Miller, J. R.; Takeuchi, E. Batteries, 1997 to 2002. *J. Electrochem. Soc.* **2004**, *151*, K1−K11.

(2) Armand, M.; Tarascon, J. Bulding better batteries. *Nature* **2008**, *451*, 652−657.

(3) Schiffer, S. H. Theory of proton-coupled electron transfer in energy conversion processes. *Acc. Chem. Res.* **2009**, *42*, 1881−1889.

(4) Serp, P.; Figuereido, J. L. *Carbon Materials for Catalysis*; John Willey & Sons: Hoboken, NJ, 2008.

(5) Costentin, C. Electrochemical approach to the mechanistic study of proton-coupled electron transfer. *Chem. Rev.* **2008**, *108*, 2145−2179.

(6) Jobic, H.; Doros, N. T. Quasi-elastic neutron scattering and molecular dynamics simulation as complementary techniques for studying diffusion in zeolites. *Microporous Mesoporous Mater.* **2007**, *102*, 21−50.

(7) Pech, D.; Brunet, M.; Durou, H.; Huang, P.; Mochalin, V.; Gogotsi, T.; Taberna, P. L.; Simon, P. Ultrahigh power micrometer-sized supercaptiors based onion-like carbon. *Nat. Nanotechnol.* **2010**, *5*, 651−654.

(8) Kuznetsov, V. L.; Chuvilin, A. L.; Butenko, Y. V.; Malkov, I. Y.; Titov, V. M. Onion-like carbon from ultra-dispersed diamond. *Chem. Phys. Lett.* **1994**, *222*, 343−348.

(9) Mamontov, E.; Herwig, K. W. A time-of-flight backscattering spectrometer at the Spallation Neutron Source, BASIS. *Rev. Sci. Intsrum.* **2011**, *82*, 085109.

(10) Singwi, K. S.; Sjölander, A. Diffusive motions in water and cold neutron scattering. *Phys. Rev.* **1960**, *119*, 863−871.

(11) Volino, F.; Dianoux, A. Neutron incoherent scattering law for diffusion in a potential of spherical symmetry: general formalism and application to diffusion inside a sphere. *Mol. Phys.* **1980**, *41*, 271−279.

(12) Volino, F.; Pineri, M.; Dianoux, A. Neutron incoherent scattering law for restricted diffusion inside a volume with an anisotropic shape. *Mol. Phys.* **1982**, *46*, 129−137.

(13) Bellissent-Funel, M.-C.; Chen, S. H.; Zanotti, J.-M. Single-particle dynamics of water molecules in confined space. *Phys. Rev. E* **1995**, *51*, 4558−4569.

(14) Stillinger, F. H. Relaxation and flow mechanisms in "fragile" glass-forming liquids. *J. Chem. Phys.* **1988**, *89*, 6461−6469.

(15) Mamontov, E.; Vlcek, L.; Wesolowski, D. J.; Cumming, P. T.; Rosenqvist, J.; Wang, W.; Cole, D. R.; Anovitz, L. M.; Gasparovic, G. Suppression of the dynamic transition in surface water at low hydration levels: a study of water on rutile. *Phys. Rev. E* **2009**, *79*, 051504.

(16) Chu, X. Q.; Ehlers, G.; Mamontov, E.; Podlesnyak, A.; Wang, W.; Wesolowski, D. J. Diffusion process in water on oxide surface: quasielastic neutron scattering study of hydration water in rutile nanopowder. *Phys. Rev. E* **2011**, *84*, 031505.

(17) Mamontov, E.; Luo, H.; Dai, S. Proton dynamics in *N,N,N,N*-tetramethylguanidinium bis(perfluoroethylsulfonyl)imide protic ionic liquid probed by quasielastic neutron scattering. *J. Phys. Chem. B* **2009**, *113*, 159−169.

(18) Mamontov, E.; Baker, G. A.; Luo, H.; Dai, S. Microscopic diffusion dynamics of silver complex-based room-temperature ionic liquids probed by quasielastic neutron scattering. *ChemPhysChem* **2011**, *12*, 944−950.

(19) Qvist, J.; Schober, H.; Halle, B. Structural dynamics of supercooled water from quasielastic neutron scattering and molecular simulations. *J. Chem. Phys.* **2011**, *134*, 144508.

(20) Sarangi, S. S.; Zhao, W.; Muller-Plathe, F.; Balasubramanian, S. Correlation between dynamic heterogeneity and local structure in a room-temperature ionic liquid: a molecular dynamics study of [bmim][PF_6]. *ChemPhysChem* **2010**, *11*, 2001−2010.

(21) Singh, R.; Monk, J.; Hung, F. R. Heterogeneity in the dynamics of the ionic liquid [$bmim^+$][PF_6^-] confined in a slit nanopore. *J. Phys. Chem. C* **2011**, *115*, 16544−16554.

(22) Mamontov, E. Diffusion in confinement as a microscopic relaxation mechanism in glass-forming liquids. *Chem. Phys. Lett.* **2012**, *530*, 55−60.